

Appendix A: Experimental Adsorption Measurements

A.1 Overview

Physical adsorption at the gas/solid interface is routinely measured in the laboratory. The most common example is found in measuring nitrogen adsorption isotherms of porous materials at 77 K between 0-100 kPa, which corresponds to the full range of P/P_0 for nitrogen (P_0 is the saturation pressure). The wide and cheap availability of nitrogen as a gas and liquid (used for cooling to 77 K) combined with its practicality as a probe molecule in determining surface area and pore size characteristics has established N₂ adsorption as a ubiquitous characterization tool and commercial instruments specifically for this purpose are widespread. In addition, commercial instruments are available for measuring the sorption of other gases such as hydrogen, carbon dioxide, and methane. Due to the complexity of these measurements and the subtleties of performing experiments across various adsorbents, adsorbates, and within different regimes of temperature and pressure, the dependability of even the most sophisticated commercial systems is inconsistent. More sophisticated apparatus and computer control typically goes along with less freedom to the scientific user. A typical pitfall is to assume that a greater number of data points may be used to overcome errors in measurement. In regimes of high temperature and pressure, systematic errors in adsorption measurement are substantial, and their effects are *cumulative*. Adsorptive

gases such as nitrogen and carbon dioxide are relatively easy to accurately measure due to larger changes in pressure and mass upon adsorption as well as typically stronger adsorption interactions. Hydrogen adsorption, on the other hand, must be measured with more care, due mainly to its lower specific uptake amounts in most materials as a result of weaker binding interactions compared to other gases (the implications for absorptive hydrogen uptake are different).

As adsorption occurs at the gas-solid interface, the weight of the solid increases and the pressure of the gas decreases. Thus, the amount adsorbed can be measured in at least two ways: by measuring the change in weight of the solid with a spring balance or measuring the change in pressure of the gas in an accurately known volume (if the volume of the sample is also known). These techniques, termed gravimetric and volumetric respectively, are summarized in Figure A.1. The resulting experimental data collected at a constant temperature, referred to as the equilibrium adsorption isotherm, is generally plotted as a function of pressure, or in some cases of P/P_0 where P_0 is the saturation vapor pressure of the adsorbate (typically at pressures below P_0):

$$n_{ads} = f(P)_T \quad (\text{generally})$$

$$n_{ads} = f\left(\frac{P}{P_0}\right)_T \quad (\text{near-saturation regime})$$

Equation A.1

Adsorption/desorption isotherms of various gases on a commercial sorbent material at different temperatures are shown in Figure A.2. The treatment of data in these distinct temperature regimes is usually different; unless otherwise noted, we will consider the case of near-critical to supercritical temperatures since this is the regime of interest for energy storage applications.

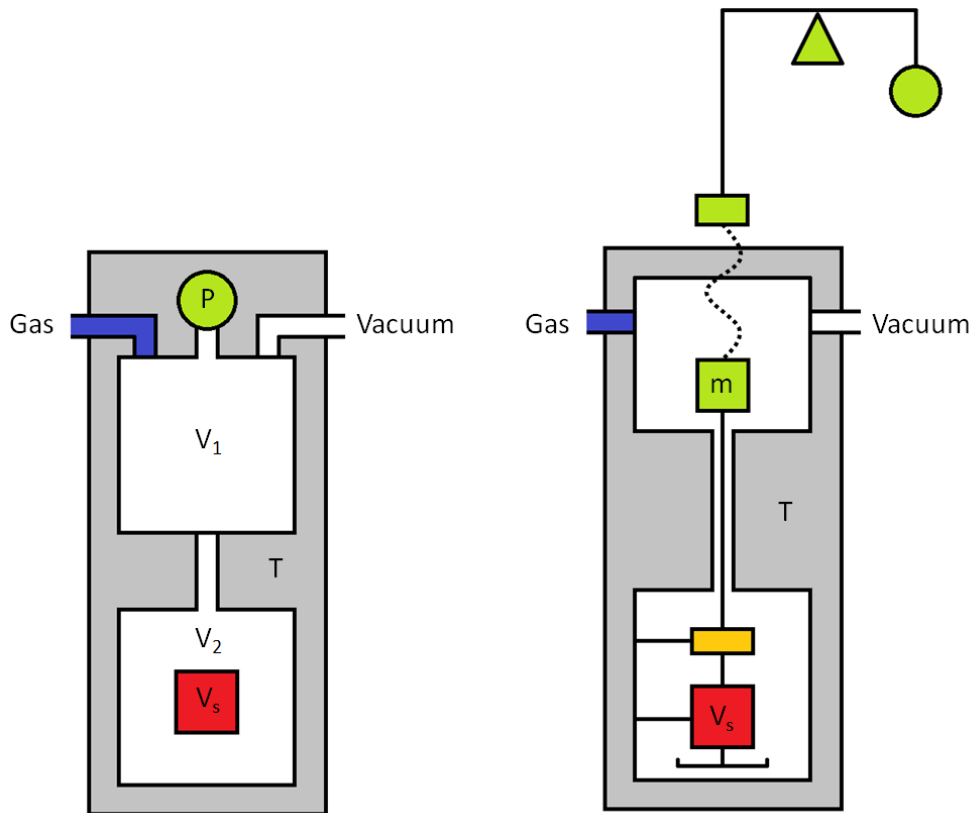


Figure A.1. Schematic representations of the volumetric (left) and gravimetric (right) methods for determining equilibrium gas-solid adsorption isotherms. In the volumetric method, pressure is measured at P before and after gas expansions between known volumes V_1 and V_2 . In the gravimetric method, the mass of the sample is measured by a suspension balance (a magnetic balance is shown) at m as pressure is increased. A second mass, shown in orange, is used for simultaneous determination of the gas density to correct for buoyancy. The primary measurement device is shown in green. The sample volume, shown in red, must be known in both cases

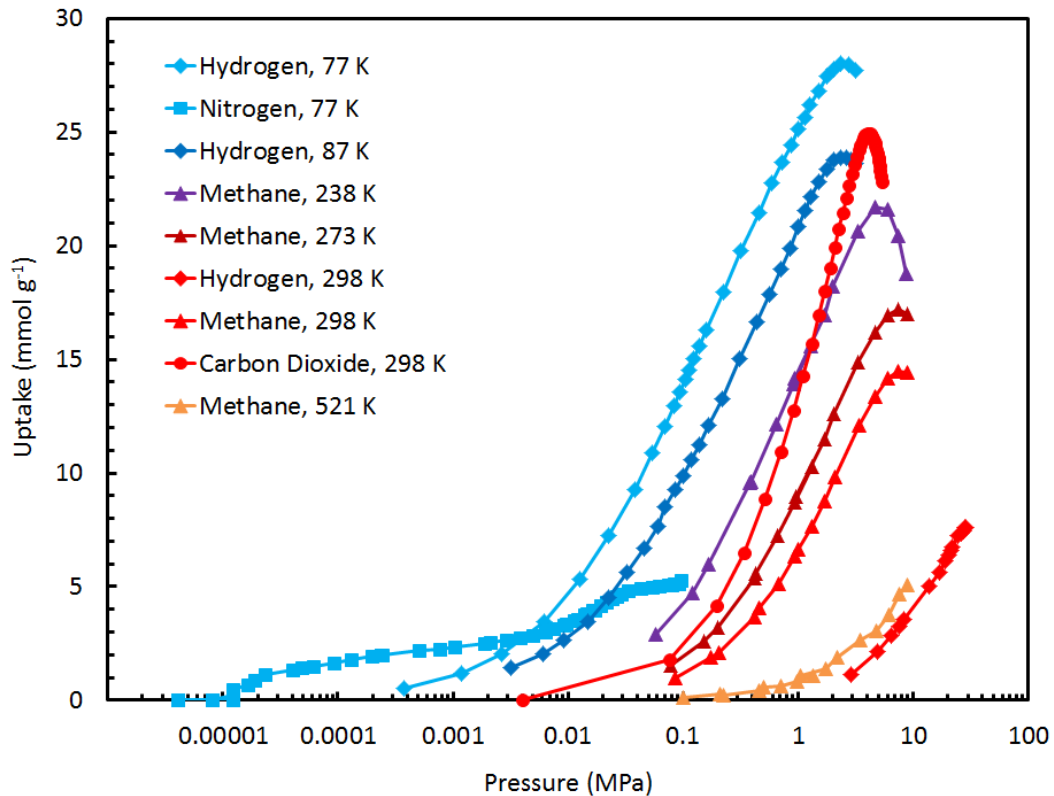


Figure A.2. Equilibrium adsorption isotherms of various adsorptive gases on a superactivated carbon, MSC-30, at temperatures between 77-521 K.

A.2 Volumetric Principles

The most common experimental technique for determining the adsorption uptake of gas by a solid material is the volumetric method. This technique is also referred to as the Sieverts method, a reference to Sieverts law which relates the concentration of gases *absorbed* in metals to pressure.¹ As the name implies, this method is also well suited to determining the absorption uptake quantities in materials.

A schematic representation of a general volumetric apparatus is shown in Figure A.3a. The simplest instrument consists of two accurately known volumes, V_1 and V_2 ,

separated by a valve, exposed to a pressure measurement device, and held at a constant temperature, T . There must be an inlet and outlet for gas. The sample, whose volume (V_s) is also known, is placed in V_2 . A practical device is shown in Figure A.3b, where only the sample environment is immersed in a controllable temperature bath while the remainder of the apparatus is held at a constant temperature near ambient. In this case, some of the free gas (corresponding to V_{bath}) will be at the bath temperature, T_{bath} , while the remainder of the apparatus will be at near ambient temperature, T_{app} . For the purposes of the following formalism, we will consider this “practical” apparatus since it is the more common (and more general) experimental setup.

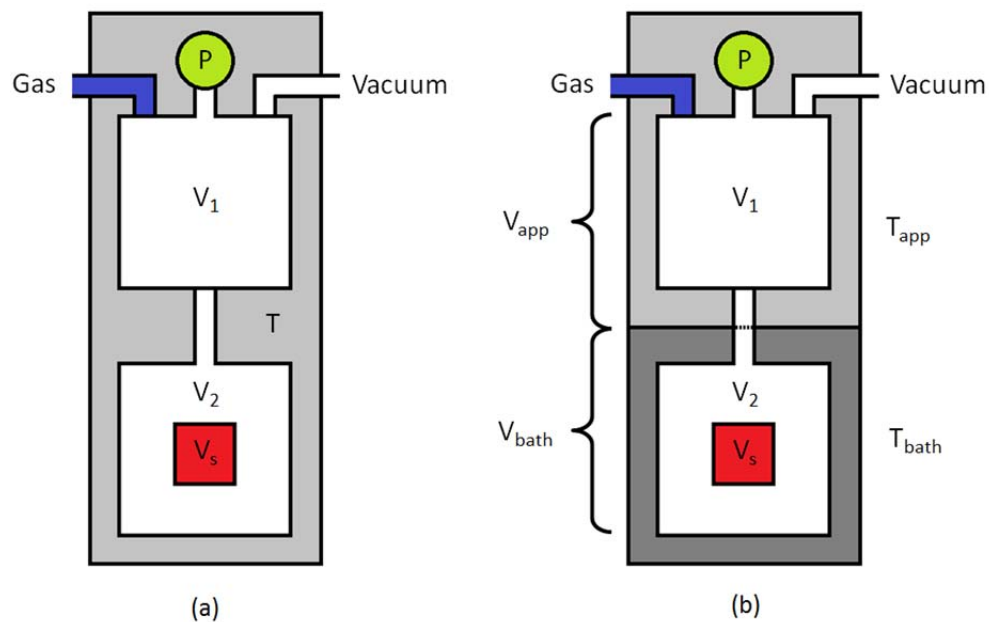


Figure A.3. The volumetric Sieverts apparatus. (a) The simplest apparatus is immersed in a constant temperature bath. (b) A more practical apparatus is held at a constant near-ambient temperature, but contains the sample and a small surrounding volume in a controllable temperature bath. The pressure is measured at P and the sample is shown in red. The areas shaded in gray represent a constant temperature region.

Measurement of a single value of the equilibrium adsorption uptake at a certain pressure and temperature requires two steps. In the first step, a specific amount of gas is confined in the “staging manifold,” V_1 . This initial amount, n_i , is the total amount of gas that will be available for adsorption in the second step. After equilibration, the dosing valve is opened and the gas is expanded into the “reactor,” V_2 , where it is exposed to the sample. After equilibration, the final amount of adsorptive remaining in the gas phase is n_f and fills a volume V_f . If we assume that the volume of the sample is independent of pressure in our experimental pressure regime (a typical assumption, suggested to be valid by both neutron diffraction measurements² and ab initio calculations³), we have the following relationships:

$$V_i = V_1$$

Equation A.2

$$V_f = V_1 + V_2 - V_s$$

Equation A.3

The temperatures of the bath and apparatus, T_{bath} and T_{app} , are held constant throughout the experiment. The temperature at the boundary between the bath and apparatus is intermediate between the two. If the volume in this intermediate region is suitably small and if the temperature control in each region is stable, we may approximate the temperature gradient between the two as a step function, so long as the ratio of the volumes of the isothermal regions, b , is accurately known. In the simplest apparatus, this approximation is not necessary. In the general case, the gaseous adsorptive in the final state occupies two isothermal volumes:

$$V_{f,app} = (1 - b) V_f$$

Equation A.4

$$V_{f,bath} = b V_f$$

Equation A.5

The equilibrium pressure before and after dosing, P_i and P_f , is measured. The density of the free gas is then determined at each step by application of the relevant gas law equation of state, and used to calculate the number of molecules in the gas phase before and after dosing, n_i and n_f , respectively:

$$n_i = \rho(P_i, T_{app}) V_i$$

Equation A.6

$$n_f = \rho(P_f, T_{app}) V_{f,app} + \rho(P_f, T_{bath}) V_{f,bath}$$

Equation A.7

If the reactor volume, V_2 , is at zero pressure before the measurement, the (excess) quantity adsorbed is simply the difference between the initial and final number of free gas molecules:

$$n_e(P_f, T_{bath}) = n_i - n_f$$

Equation A.8

The amount adsorbed is reported as a function of the final conditions in the sample environment. Repeated points are measured in this way at different equilibrium pressures to construct an adsorption uptake isotherm at the constant temperature T_{bath} . If the pressure in V_2 is returned to zero between points, the calculated uptake at the x^{th} point is always the same:

$$n_{e,x}(P_f, T_{bath}) = n_{i,x} - n_{f,x}$$

Equation A.9

If a cumulative measurement is desired, the cumulative uptake may be measured at each point by taking into account that the final pressure from the previous point is the starting pressure in the reactor. The final free gas density in each temperature region of V_2 must be multiplied by its respective volume ($V_{2,app}$ and $V_{2,bath}$) and added to the new free gas dose to get the total initial amount of adsorptive:

$$n_{i,cum,x} = \rho(P_{i,x}, T_{app})V_i + \rho(P_{f,x-1}, T_{app})V_{2,app} + \rho(P_{f,x-1}, T_{bath})V_{2,bath}$$

$$\Delta n_{e,x}(P_f, T_{bath}) = n_{i,cum,x} - n_{f,x}$$

$$n_{e,x}(P_f, T_{bath}) = n_{e,x-1} + \Delta n_{e,x}$$

Together, the series of points $n_{e,x}$ are used to find the function f :

$$n_e = f(P)_T = f(P_f)_{T_{bath}}$$

Equation A.10

A schematic of the procedure corresponding to the cumulative measurement of two adsorption points by the volumetric method is shown in Figure A.4. Equilibrium desorption isotherms are measured in a similar way. In the initial step, there is a high pressure in the reactor and a lower pressure (or zero pressure) in the staging manifold. It is helpful to have an additional pressure gauge in the reactor volume, but is not necessary.

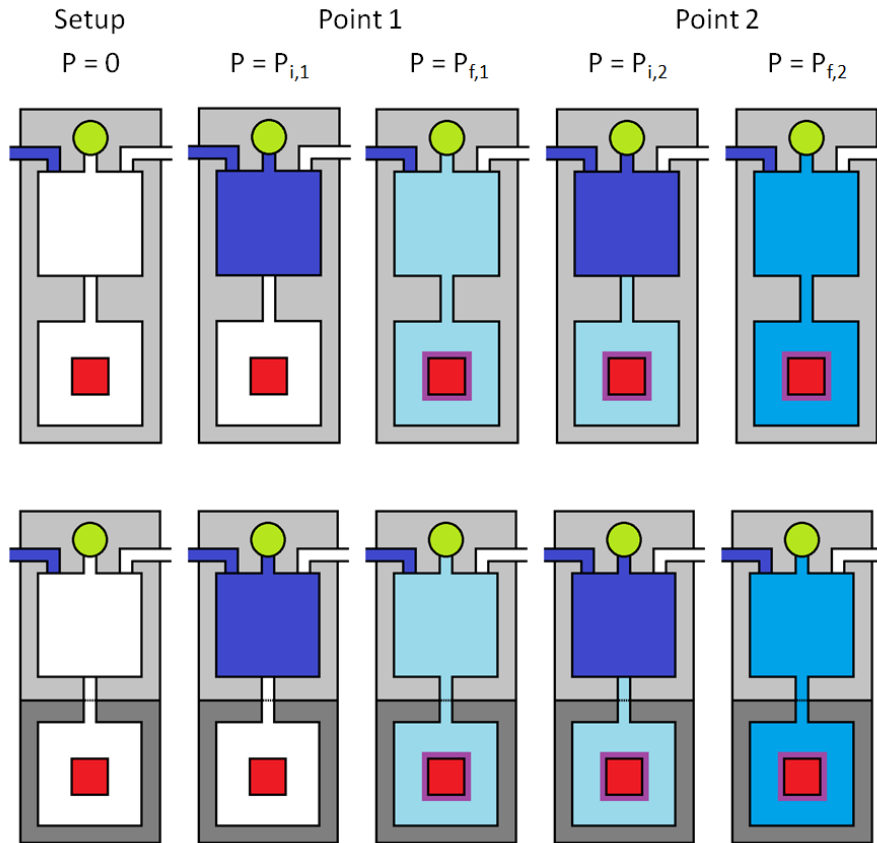


Figure A.4. The schematic representation of a 2 point dosing sequence during volumetric measurement of adsorption uptake, involving 2 steps at each point. The sequence is shown for increasing pressure steps from left to right. The top sequence corresponds to the simplest Sieverts apparatus, and the bottom corresponds to a practical apparatus. The pressure measured at each step is shown above.

Appendix B: Further Results Concerning Hydrogen Spillover

A response^{4 5} to our study presented in Chapter 3 opined that our materials were incorrectly synthesized, specifically questioning the nanoparticle dispersion and size. Attempts were made to compare TEM micrographs between materials, but this method of comparison is highly subject to bias in the region chosen. We suggest that a more accurate comparison be made by direct overlay of the XRD data of both materials, shown in Figure B.1. It can be seen that no significant difference, except possibly a *larger* mean particle size in Pt/AX-21⁶, can be observed between it and Pt-MS-30. The sharp peaks in the XRD data of Pt/AX-21 are not consistent with a Lorentzian shape and indicate the likelihood of a contribution by even larger particles as well. Both platinum-doped materials are confirmed to contain particles of diameter < 2 nm by TEM studies, but the distribution of particle sizes undoubtedly includes small particles as well as larger particles; we expect that if it was an important mechanism in overall uptake, enhancement due to spillover would be apparent in Pt-MS-30 to a measurable extent.

Other points that should be addressed include:

- 1) The degas temperature used for Pt-MS-30 was simply misstated, not incorrectly performed. The actual temperature of degas used in our studies was 623 K.
- 2) The Pt-content is ~30% higher in Pt-MS-30 than Pt/AX-21, causing a more dramatic change in surface area upon doping. While the trend of decreased

spillover enhancement with increased catalyst loading was reported by Saha et al.⁷ and Zieliński et al.⁸, this was only for Ni particles in both cases. In fact, Saha reports that for Pt particles on OMC, spillover enhancement increased with Pt loading (up to 10 wt%). Enhancement due to spillover should still be measurable in Pt-MSC-30 if it plays an important role in overall hydrogen uptake. Furthermore, substantial (unexplained) hysteresis in the uptake measurements reported by Saha et al. is highly indicative of the type of error accumulation we have eliminated in our data by increasing sample size.

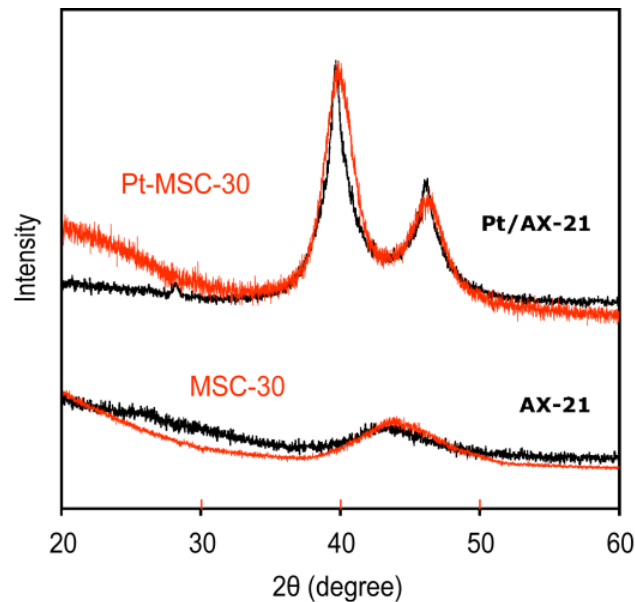


Figure B.1. XRD patterns of MSC-30 and Pt-MSC-30 (from this work) compared to Pt/AX-21 and AX-21.⁶

Further studies of the hydrogen spillover phenomenon and its role in hydrogen storage have been performed since our report. The experimental results can be

summarized by stating that uptake enhancement due to spillover is less than was originally reported in 2000-2007. Efforts to standardize the results have been undertaken by NIST. To control for differences in materials preparation, etc., the same samples were distributed to numerous groups for uptake measurements. We received a blind set of samples, used the specific degas protocols described by NIST, and contributed the results shown in Figure B.2. While the identity of the materials is not known to us, the results do show an appreciably higher hydrogen uptake capacity in Sample 2 (indicating the likelihood that Sample 1 is the standard and Sample 2 is the spillover material). However, the uptake in Sample 2 was not reversible at room temperature and desorption of hydrogen from the spillover sample was $\sim 0.3 \text{ mmol g}^{-1}$, the same as in the pure carbon precursor. In addition, we studied the kinetics of possible hydrogen uptake by spillover, yielding the results shown in Figure B.3. After 2 hours of exposure to hydrogen at an equilibrium pressure of $\sim 0.7 \text{ MPa}$, the measured pressure in the sample container was essentially constant within the limits of transducer resolution, indicating no significant ongoing adsorption associated with spillover. The temperature signal, converted to an effective pressure (from the assumption of constant volume and mass) can also be used to estimate changes in the thermodynamic state of the system: the rise of 0.5-1 Torr-equivalent of pressure as measured by temperature indicates that a maximum of $\sim 1 \text{ Torr}$ (0.1 kPa) may have left the gas phase over the course of the 2 hours, corresponding to 10^{-6} mol H_2 , or $\sim 2\%$ of the total hydrogen adsorbed. We suggest this as an approximation of the limit of spillover contribution to hydrogen storage in this material.

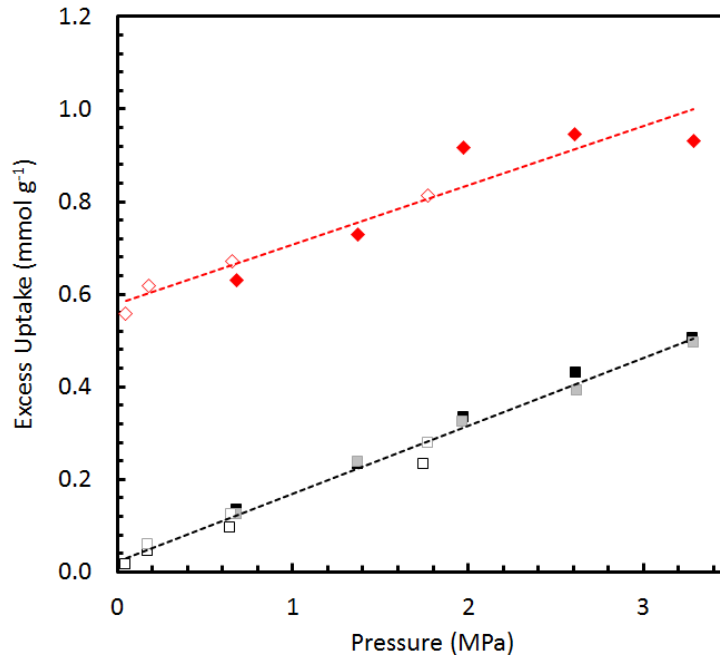


Figure B.2. Hydrogen adsorption isotherms (filled markers) of a sample of spillover-catalyst doped carbon “#2” (red) and its pure carbon precursor “#1” (black and gray) between 0-3.5 MPa at 298 K, showing a measurable increase in uptake in the spillover material. Reversible desorption (empty markers) is also shown.

The combined results from the entire multi-group NIST study led to the following conclusions:

- 1) The maximum uptake capacity of spillover materials is < 1 wt%, or 5 mmol g⁻¹, at 298 K, significantly below the original reports for Pt/AX-21 and IRMOF-8.
- 2) The presence of palladium nanoparticles is itself responsible for up to 30% enhancement in those materials, and the amount of enhanced hydrogen sorption by hydride formed should be subtracted from the capacity attributed to spillover.

- 3) The measurable enhancement of hydrogen uptake attributed to spillover ranged from 0-50% despite rigorous attempts to control sample quality.
- 4) The degassing temperature is considered a crucial step for proper sample preparation, and reversibility was an unresolved issue across all samples.

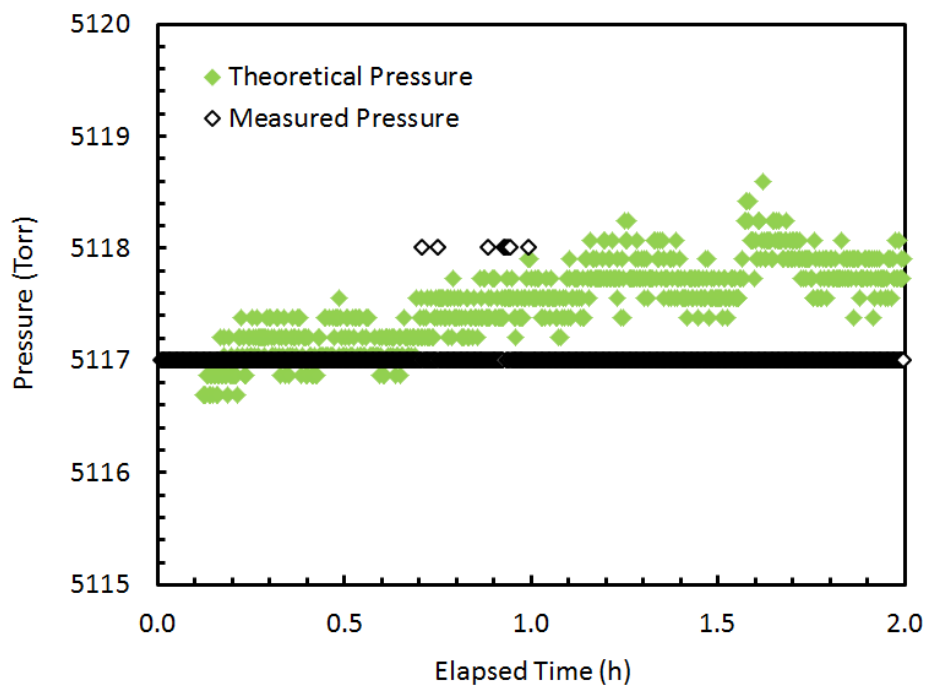


Figure B.3. The temperature and pressure data, shown in units of Torr, during an adsorption measurement step in sample #2, a spillover-catalyst decorated carbon, at 298 K and ~ 0.7 MPa. The difference in the signals from pressure (black unfilled diamond) and temperature (green diamond) could potentially be attributed to ongoing spillover, corresponding to 2% of the total uptake at this step: 0.01 wt% H_2 .

Appendix C: Carbon Dioxide Adsorption on ZTCs

During the studies of gas adsorption on ZTCs, carbon dioxide measurements were performed in addition to the N_2 , H_2 , and CH_4 isotherms presented in Chapters 4-5. The results are presented in Figures C.1-2.

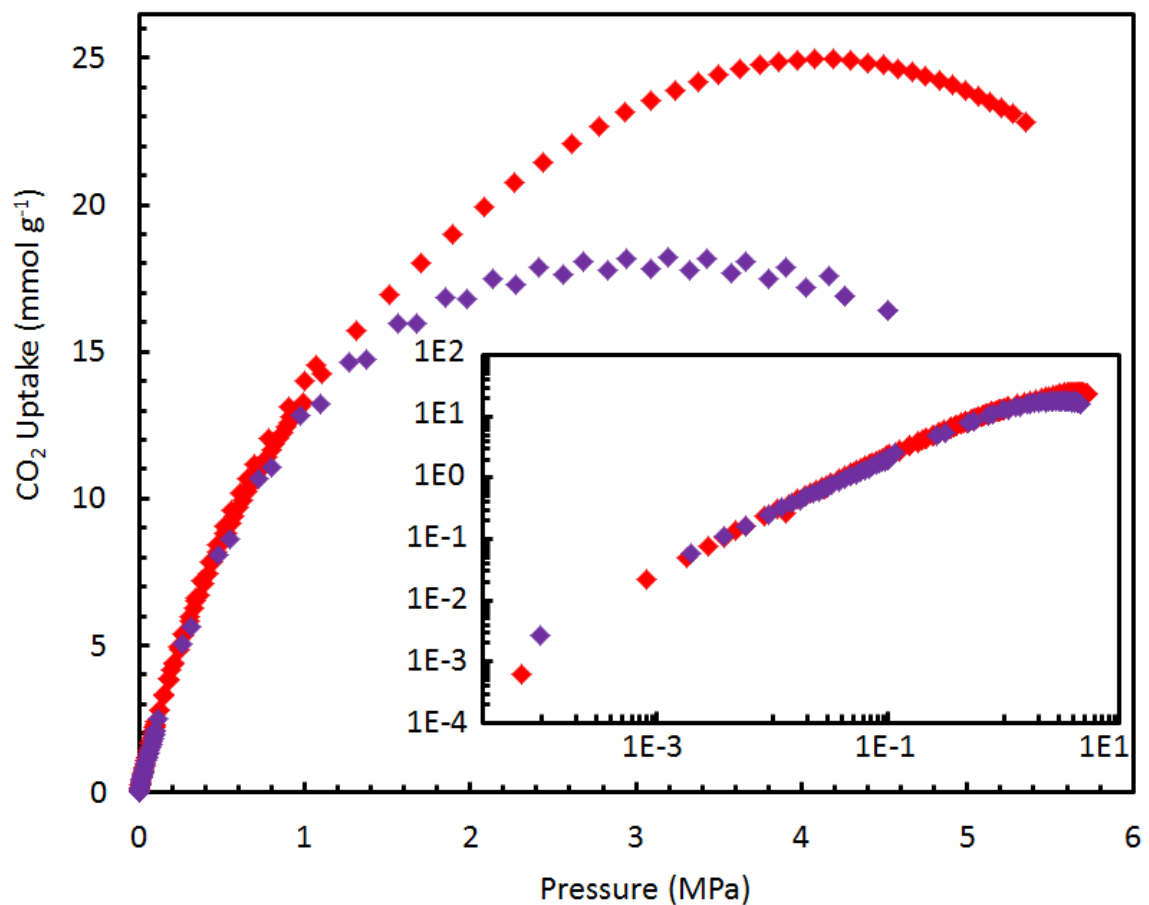


Figure C.1. Equilibrium excess adsorption isotherms of carbon dioxide on ZTC-2 (purple) and MSC-30 (red) at 298 K.

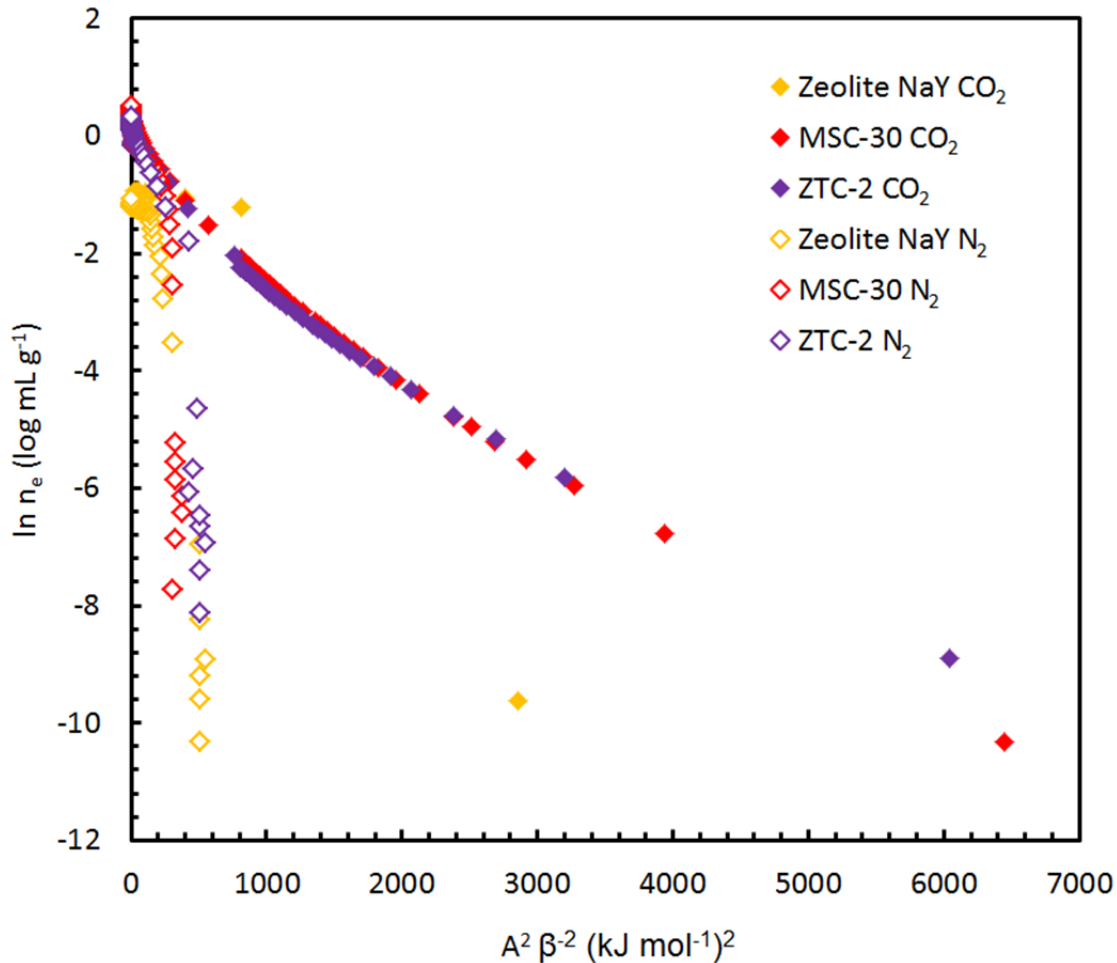


Figure C.2. Characteristic curves of N_2 (unfilled diamonds, 77 K) and CO_2 (solid diamonds, 298 K) adsorption on zeolite NaY (yellow), MSC-30 (red), and ZTC-2 (purple).

The results remain unclear, and not enough data was collected. However, it appears that while CO_2 adsorption at 298 K was similar between MSC-30 and ZTC-2, N_2 adsorption at 77 K was significantly different between them. It is interesting to note that N_2 adsorption in ZTC-2 and its raw zeolite template (NaY) show similar behavior at low pressure (where low pressure corresponds to large A^2/β^2 in the “characteristic curve”⁹). Further work remains to be done, and it is likely that more promising results could be obtained with the higher fidelity ZTC sample, ZTC-3.

Appendix D: BET and DR Trends of Adsorption Uptake

We have routinely performed Dubinin-Radushkevich¹⁰ (DR) analyses on adsorbent materials to determine if there is a different trend than for BET surface area, and typically did not find a different result (see Figure D.1). Owing to its wider use and acceptance, the BET method was chosen for the results presented throughout this work.

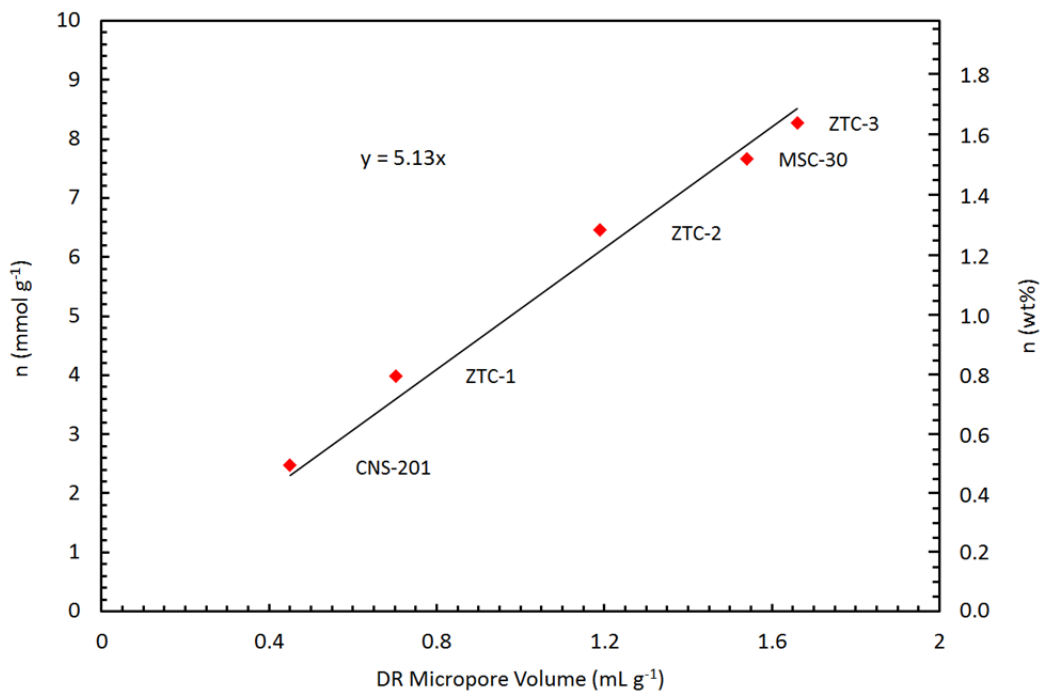


Figure D.1. Excess hydrogen uptake at 30 MPa and 298 K for various carbon materials as a function of DR micropore volume.

Appendix E: Pressure Driven Phase Transition

During gas adsorption measurements, gas is expanded through a valve into the sample container, as described in Appendix A. A fixed amount of gas, expanded from an initial pressure P_i , will equilibrate with the adsorbent at pressure P_f , determined by the properties of the adsorbent and the ratio of the final volume to the initial volume, $x = V_i/V_f$. Compared to an identical non-adsorption reference case, expansion of gas into a container filled with adsorbent results in a lower pressure and a lower free energy from solid-adsorbate interactions. This difference in pressure between the reference state and the adsorption system corresponds to a difference in chemical potential given by:

$$\Delta\mu_{ads}(P_i, P_f) = \mu(P_f, T) - \mu(P_i, T)$$

Equation E.1

The thermodynamic driving force for adsorption can be interpreted as this change in chemical potential. The larger the surface available for adsorption, and hence the more adsorptive molecules that can depart the gas phase to undergo adsorption, the larger the change in free energy of the system. In a carefully designed experiment, this potential difference can drive a phase transition of an adsorbent material to a lower free energy state where more binding sites are available for adsorption. The nature of the chemical potential in the non-ideal gas region for hydrogen and methane is different (see Figure 6.3).

As described in Section 6.2.2, this final state would be energetically favorable since adsorption interactions would lower the total free energy below that of the bound state. For carbon nanotubes, this corresponds to the separation of bundles to expose the full surface of the individual tubes, represented in Figure E.1. A series of TEM images (Figure E.2) verify the initial, bundled state of single-walled nanotubes obtained in early investigations.

With an adsorption isotherm measurement at temperature T , it is possible to derive the relationship between P_i and P_f for a specific amount of adsorbent in a given void volume if the adsorption isotherm is known. The change in chemical potential is unique to the experimental setup since the pressure change is dependent on the volume; for a large volume relative to the amount of adsorbent, the change in chemical potential will be small since the pressure drop associated with adsorption is small. However, with carefully chosen experimental conditions, one can effect a substantial decrease in chemical potential with the addition of a high surface for adsorption to an empty container. Initial calculations of the effective chemical potential that could be applied for different experimental conditions are shown in Figures E.3-4. Numerous simplifying approximations were used in order to predict the final pressure based on experimental excess hydrogen and methane adsorption uptake measured of MSC-30 compared to CNS-201. A key step was to assume that the bundled structures have a surface area 5% that of MSC-30 ($150 \text{ m}^2 \text{ g}^{-1}$), and therefore 5% the excess maximum uptake before phase transition. After phase transition, the surface area was approximated to grow 10 fold. This is the maximum increase given the geometry of a typical bundle of 7 tubes.

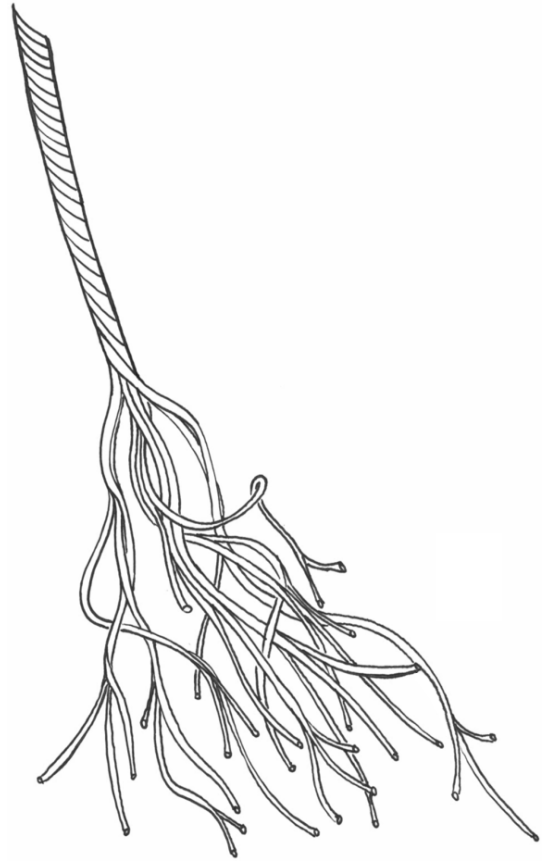
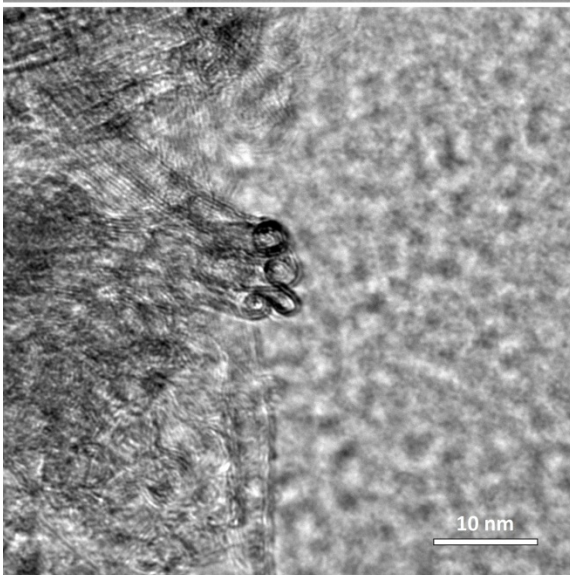
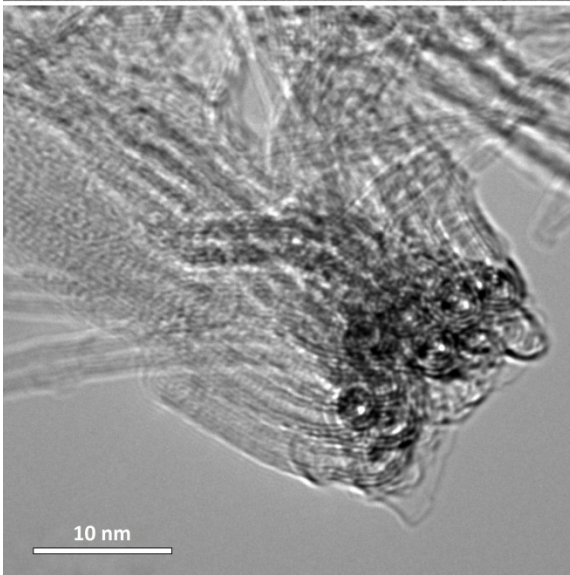
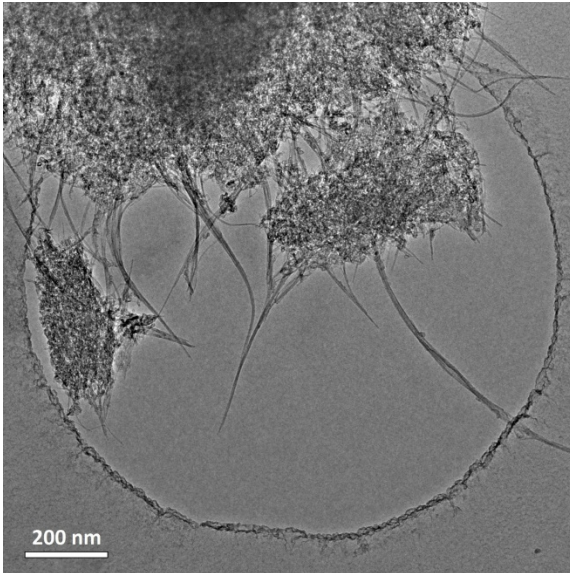


Figure E.1. (above) An artistic representation of the un-bundling of the rope structure of single-walled carbon nanotubes.

Figure E.2. (left) TEM micrographs of single-walled carbon nanotubes over a holey-carbon grid, showing their bundled structure.

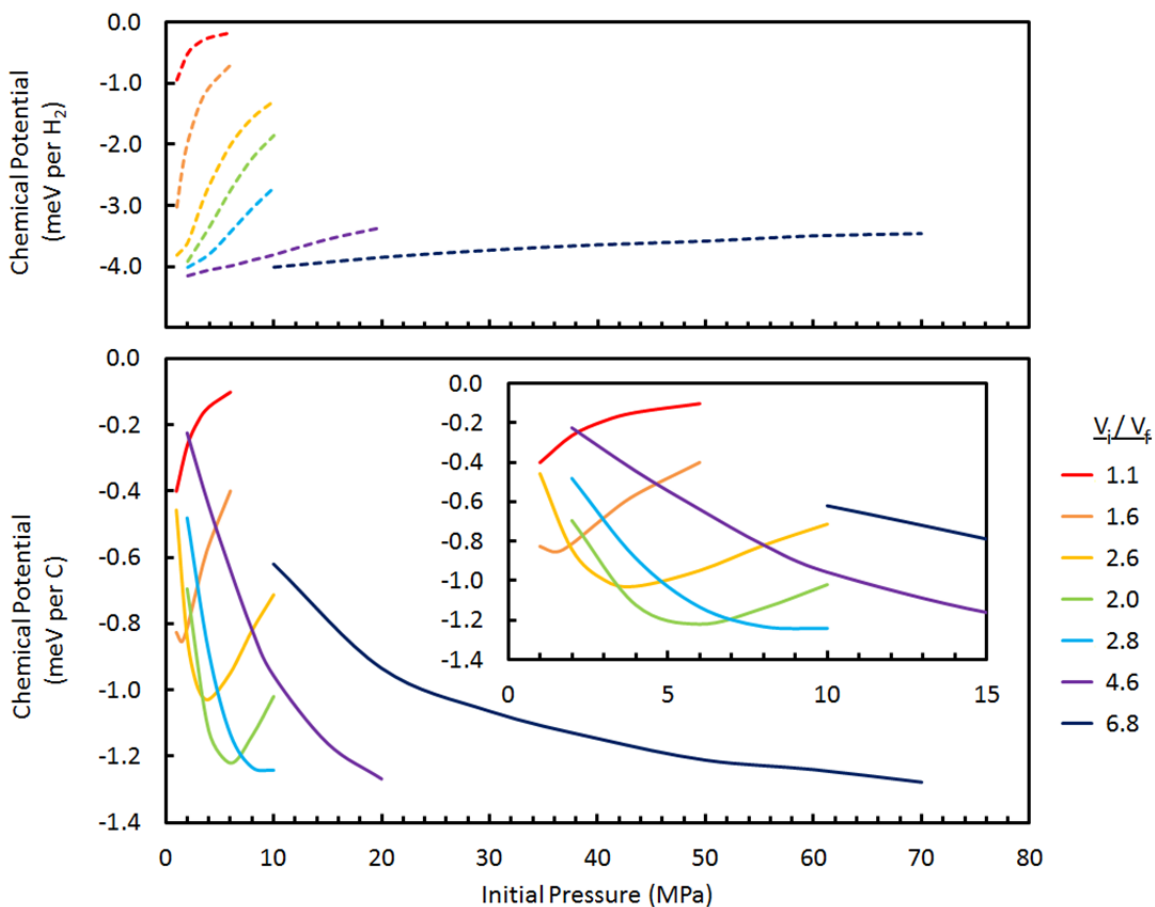


Figure E.3. (top) The change in chemical potential after a 1-step hydrogen expansion between 2 fixed volumes, one containing adsorbent, in a temperature bath held at 77 K, and (bottom) the corresponding effective change per carbon atom (a function of surface coverage) in seven different apparatuses with total volumes: 51 mL (red), 17 mL (orange), 10 mL (yellow), 2 L (green), 32 mL (light blue), 23 mL (purple), and 1 L (dark blue).

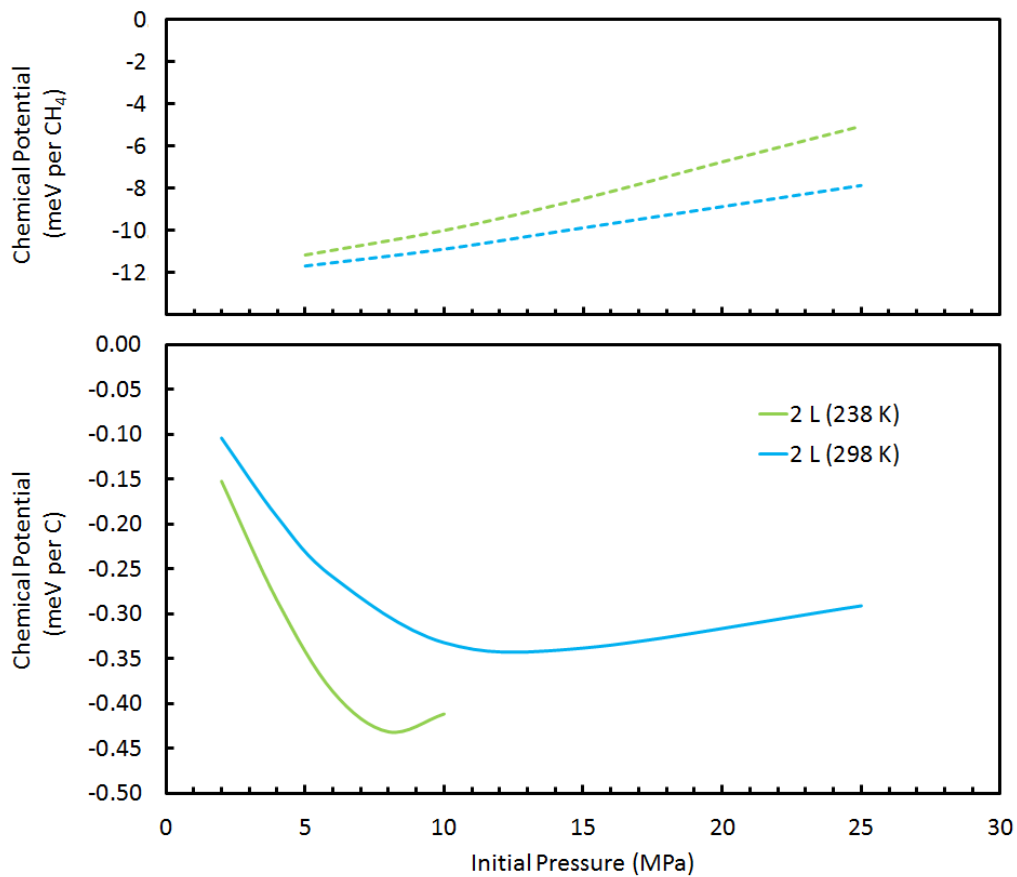


Figure E.4. (top) The change in chemical potential after a 1-step methane expansion between 2 fixed volumes, one containing adsorbent, in a fixed temperature bath, and (bottom) the corresponding effective change per carbon atom (a function of surface coverage), in the same model apparatus (2 L total volume) at two temperatures: 238 K (green) and 298 K (blue).

Appendices References

- (1) A. Sieverts, 'Die aufnahme von gasen durch metalle', *Z. Metallkd.*, **21**, 37-46 (1929).
- (2) H. Wu, W. Zhou, and T. Yildirim, 'High-capacity methane storage in metal-organic frameworks M2(dhtp): the important role of open metal sites', *J. Am. Chem. Soc.*, **131**, 4995-5000 (2009).
- (3) K. Sillar and J. Sauer, 'Ab initio prediction of adsorption isotherms for small molecules in metal-organic frameworks: the effect of lateral interactions for methane/CPO-27-Mg', *J. Am. Chem. Soc.*, doi: 10.1021/ja307076t (2012).
- (4) N. R. Stuckert, L. Wang, and R. T. Yang, 'Characteristics of hydrogen storage by spillover on Pt-doped carbon and catalyst-bridged metal organic framework', *Langmuir*, **26**, 11963-11971 (2010).
- (5) H. Chen and R. T. Yang, 'Catalytic effects of TiF3 on hydrogen spillover on Pt/carbon for hydrogen storage', *Langmuir*, **26**, 15394-15398 (2010).
- (6) Y. Li and R. T. Yang, 'Hydrogen storage on platinum nanoparticles doped on superactivated carbon', *J. Phys. Chem. C*, **111**, 11086-11094 (2007).
- (7) D. Saha and S. Deng, 'Hydrogen adsorption on ordered mesoporous carbons doped with Pd, Pt, Ni, and Ru', *Langmuir*, **25**, 12550-12560 (2009).
- (8) M. Zieliński, R. Wojcieszak, S. Monteverdi, M. Mercy, and M. M. Bettahar, 'Hydrogen storage in nickel catalysts supported on activated carbon', *Int. J. Hydrogen Energy*, **32**, 1024-1032 (2007).
- (9) D. Cazorla-Amorós, J. Alcañiz-Monge, and A. Linares-Solano, 'Characterization of activated carbon fibers by CO2 adsorption', *Langmuir*, **12**, 2820-2824 (1996).
- (10) S. J. Gregg and K. S. W. Sing, *Adsorption, surface area, and porosity*, Academic Press, London (1982).